J Mater Sci (2011) 46:902–909
DOI 10.1007/s10853-010-4833-5

Reactive sintering mechanism of Ti + Mo_2C and Ti + VC powder compacts

Yan Bin Liu · Yong Liu · Hui Ping Tang · Bin Wang · Bin Liu

Received: 15 March 2010 / Accepted: 14 August 2010 / Published online: 2 September 2010

Abstract TiC reinforced Ti-matrix composites have been synthesized successfully by reactive sintering of Ti-1.5%Fe-2.25%Mo (wt%) powder compacts with addition of Mo_2C and VC particles. The reactions for the formation of TiC particles start at 600 °C, but the distribution of TiC particles and the densification behavior in the two compacts are significantly influenced by the metal carbides (Mo_2C or VC). The compact with addition of Mo_2C has a relative density of 98% after sintering at 1300 °C for 1.5 h, but TiC particles are agglomerated in the Ti matrix. The compact with addition of VC has a relative density of about 91% after sintering at 1300 °C for 1.5 h, but TiC particles distribute more homogenously in the Ti matrix. Different TiC particle distribution and densification behaviors are attributed to the reaction rates between Ti and metal carbides and the subsequent diffusion process.

Introduction

In situ particulate reinforced titanium matrix composites (TMCs) offer a combination of good mechanical properties and high-temperature stability, and are attractive materials for automotive, aerospace, and military applications [1–4]. One of the most promising reinforcing particles is TiC due to its good thermal and chemical compatibility with the Ti matrix [2–4]. Various methods such as self-propagating high-temperature synthesis [5, 6], mechanical alloying [7], powder metallurgy [4, 8–11], and casting [2] have been utilized to prepare in situ TiC particle reinforced TMCs for structural applications. Among these methods, the blended elemental powder metallurgy method is desirable as it has the potential to produce low-cost TMCs parts. The commonly used carbon sources of in situ TiC reinforced TMCs are graphite powder, B_4C powder, or flowing methane [4, 8–11]. It has been reported that the reactive sintering of a multi-component powder mixture of titanium powder and transition metal carbide (Cr_2C_3) can not only form in situ TiC particles to enhance the Ti matrix, but also stabilize the β phase by the chromium element to improve the elongation-to-failure of the Ti matrix [3, 12, 13]. It is hence reasonable to expect that the reactive sintering of Ti and metal carbides with β phase-stabilizing elements can improve the mechanical properties of in situ TiC reinforced TMCs. Since various chemical reactions take place during the reactive sintering process due to different starting reactants, the compositions and microstructures of TMCs are quite different from each other [8–11]. However, the effects of reactant powders and processing parameters on the microstructural evolutions of the TMCs have not been well understood. The aim of this article is to investigate the reactive sintering behavior of Ti-1.5%Fe-2.25%Mo (wt%) powder compact with addition of two different types of metal carbide (Mo_2C and VC).

Experimental

Ti powder (<104 μm), Fe powder (4 μm), Mo powder (5 μm), Mo_2C powder (<2 μm), and VC powder (<2 μm)

Y. B. Liu · Y. Liu (✉) · B. Wang · B. Liu
State Key Laboratory of Powder Metallurgy, Central South University, Changsha 410083, People's Republic of China
e-mail: yonliu11@yahoo.com.cn

H. P. Tang
State Key Laboratory of Porous Metals, Northwestern Research Institute of Nonferrous Metals, Xi'an 710012, People's Republic of China

were blended according to the compositions of Ti-1.5%Fe-2.25%Mo-12%Mo_2C (Ti + Mo_2C) and Ti-1.5%Fe-2.25% Mo-6%VC (wt%) (Ti + VC), respectively. The weight percentages of the metal carbides added in the mixtures were designed to obtain a similar volume fraction (~5%) of TiC particles. The mixtures were first cold pressed into cylinders of Ø12 × 100 mm at a pressure of 400 MPa, then sintered at various temperature of 850, 1000, 1150, and 1300 °C for 1.5 h under a vacuum of 5×10^{-3} Pa, and finally cooled in the furnace. The tensile tests were carried out on a CSS-4400 test machine using carefully polished specimens with a gauge size of Ø5 × 25 mm. Densities were determined by the Archimedes method. The thermal behavior of the sintering process for the compacts was studied by NETZSCH STA 449C differential scanning calorimetry (DSC). The microstructures of the compacts after sintering at different temperatures were investigated by optical microscopy (OM) and scanning electron microscopy (SEM) in the backscattered mode (BSE). X-ray diffraction (XRD) analysis was conducted to determine the phase constitutions. The composition of different phases was determined by energy-dispersive spectrometer (EDS) attached to the SEM.

Results

Thermodynamics calculation

The reactions between titanium and Mo_2C, VC are designed as follows:

$$Ti + Mo_2C = TiC + 2Ti(Mo) \quad (1)$$

$$Ti + VC = TiC + Ti(V) \quad (2)$$

The thermodynamic feasibility of in situ reactions involved in this study has been calculated using the thermodynamic data from [14]. The changes of Gibbs free energy, ΔG, increase slightly with the reaction temperature increase from 400 to 1400 °C. All ΔGs are negative, indicating that the reactions (1) and (2) for the synthesis of TiC are thermodynamically feasible. It is also found that the reaction between Ti and Mo_2C has a higher driving force than that between Ti and VC.

Thermal behavior

Figure 1 shows the DSC curves for Ti + Mo_2C and Ti + VC compacts. It can be seen that the DSC curves of both compacts change from endothermic to exothermic at about 600 °C, implying the start of the reactions between Ti and metal carbides. The endothermic peaks appearing at about 900 °C can be attributed to the phase transformation

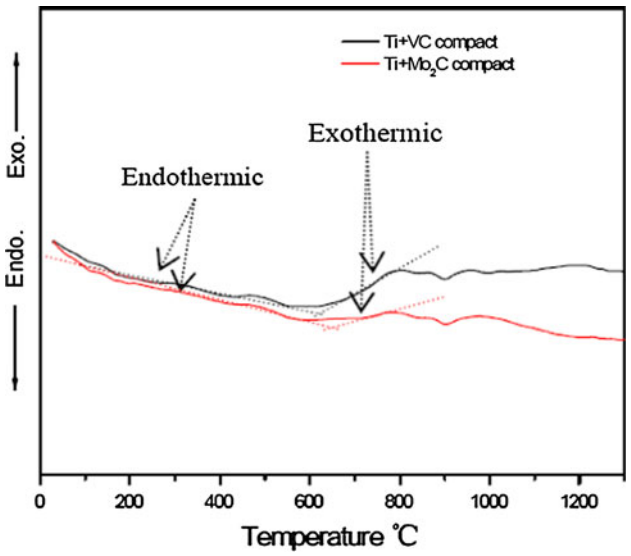

Fig. 1 DSC curves for Ti + Mo_2C and Ti + VC compacts

of $\alpha \rightarrow \beta$. Furthermore, no other apparent endothermic peaks can be found in the DSC curves.

Phase constitution

Figures 2 and 3 show the XRD patterns for the Ti + Mo_2C and Ti + VC compacts after sintering at 850, 1000, 1150, and 1300 °C for 1.5 h, respectively. For comparison, the patterns for the cold pressed compacts are also shown. The peaks corresponding to raw powders of Ti, Mo_2C, and VC can be clearly observed in the compacts, but the peaks corresponding to elemental Fe and Mo powders are not detected due to their small amount. The XRD patterns in Fig. 2 for Ti + Mo_2C compact after sintering at 850 °C for 1.5 h show new peaks of Mo, TiC, and β-Ti, as well as the disappearance of the peaks of Mo_2C. With increasing sintering

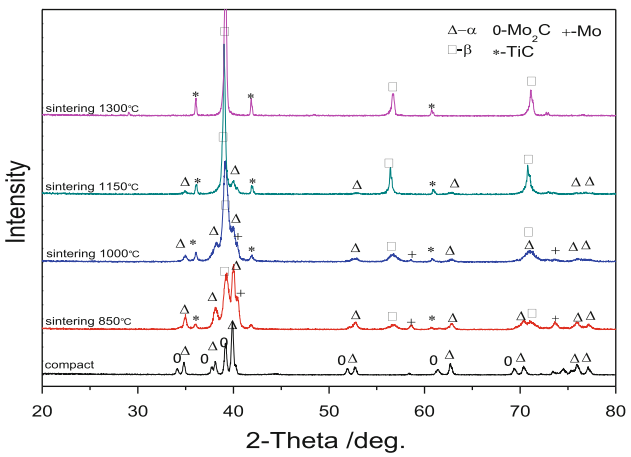

Fig. 2 X-ray diffraction patterns corresponding to the Ti + Mo_2C compacts after sintering at different temperatures

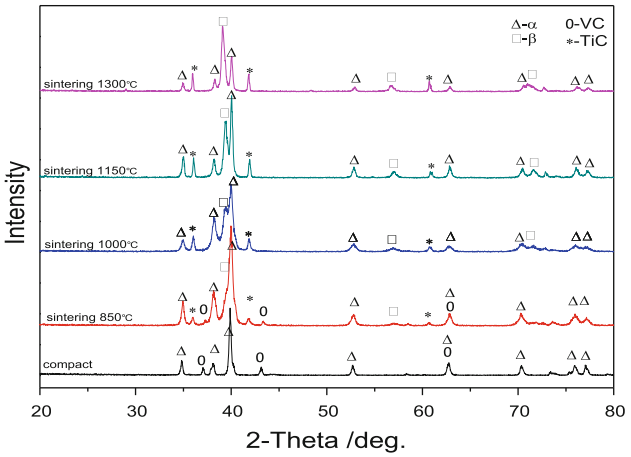

Fig. 3 X-ray diffraction patterns corresponding to the Ti + VC compacts after sintering at different temperatures

temperature from 850 to 1300 °C, the peak intensities corresponding to β-Ti and TiC increase, while the peak intensities of α-Ti and Mo gradually decrease and at last disappear after sintering at 1300 °C for 1.5 h. The XRD patterns in Fig. 3 show the co-existence of VC and newly formed TiC for Ti + VC compact after sintering at 850 °C for 1.5 h. The formation of β-Ti phase in the compact is also observed. Increasing the sintering temperature to 1000 °C leads to complete consumption of VC and increased amount of β-Ti and TiC. With the temperature continuously increasing to 1300 °C, the peak intensities corresponding to β-Ti and TiC in the XRD patterns increase, while the peak intensities of α-Ti gradually decrease.

Microstructural evolution

The microstructure of the Ti + Mo_2C compact after sintering at 850 °C for 1.5 h is shown in Fig. 4. Three areas marked as A, B, and C with distinct contrast can be clearly seen from Fig. 4a, b. EDS analysis shows that area A is the core of an un-reacted Ti particle (Fig. 4c), and the outer layer of the Ti particle, marked as B, is rich in carbon, Mo, and Fe (Fig. 4d). Tiny TiC particles are also seen in the reacted layer of the Ti particle. The white area, marked as C, in the edge of Ti particles is rich in Mo, which also contains a small amount of carbon and Ti (Fig. 4e). After sintering at 1000 °C for 1.5 h, only a small amount of Mo-rich areas remains in the edges of primary Ti particles, as shown in Fig. 5a. A Widmanstätten ($\alpha + \beta$) structure is formed in the centers of Ti particles, and the TiC particles become inhomogeneous in the Ti-matrix (Fig. 5a). As the sintering temperature increases to 1150 and 1300 °C, the distribution of TiC particles becomes obviously more inhomogeneous, as shown in Fig. 5b, c. The alloying elements Fe and Mo are completely dissolved into the Ti particles at the above temperatures.

Figure 6 presents the microstructure of the Ti + VC compact after sintering at 850 °C for 1.5 h. It is shown that the outer layers of the primary Ti particles have reacted with VC, and are rich in carbon, Mo, V, and Fe elements. The reacted layers are much thinner than those in the Ti + Mo_2C compact sintered at the same temperature, and less amount of TiC particles is observed in these layers. The un-reacted VC together with some Mo and Ti remain on edges of the Ti particles. At 1000 °C, the Ti particles are almost fully consumed by the reacted layers, and exhibit a $\alpha + \beta$ lamellar structure. Equiaxed TiC particles with a size varying from 5 to 8 μm are formed and homogeneously distributed in the matrix, as seen from Fig. 7a. With the temperature increasing to 1150 and 1300 °C, there is no significant change of the microstructures for the Ti + VC compact, except for the slight growth of TiC particles (Fig. 7b, c).

Density and mechanical properties

The optical micrographs of the Ti + Mo_2C and Ti + VC compacts after sintering at 850 °C for 1.5 h are shown in Fig. 8. It is clearly seen that sintering necks can form more easily in the Ti + Mo_2C compact than in the Ti + VC compact, and large pores remain in the Ti + VC compact. The relative densities of the two types of compact after sintering at different temperatures are shown in Fig. 9. It may be noted that the densities of the Ti + Mo_2C compacts are higher than those of the Ti + VC compacts under all sintering temperatures. The mechanical properties of the compacts after sintering at 1300 °C for 1.5 h measured by tensile tests are listed in Table 1. As can be seen, the Ti + Mo_2C compact has a higher tensile strength and yield strength than the Ti + VC compact, but the ductilities of both compacts are at a relative low level.

Fractography

The fracture surfaces of the compacts after sintering at 1300 °C for 1.5 h are shown in Fig. 10. The important features include the coalescence of microvoid in the matrix, as well as flat facets of fractured particles. Also, there are residual pores in the fracture surfaces, and the amount is larger in Ti + VC compact than in Ti + Mo_2C compact.

Discussion

Reactive sintering mechanism

As seen from Fig. 1, no apparent exothermic peak can be found in the DSC curves, which may be attributed to

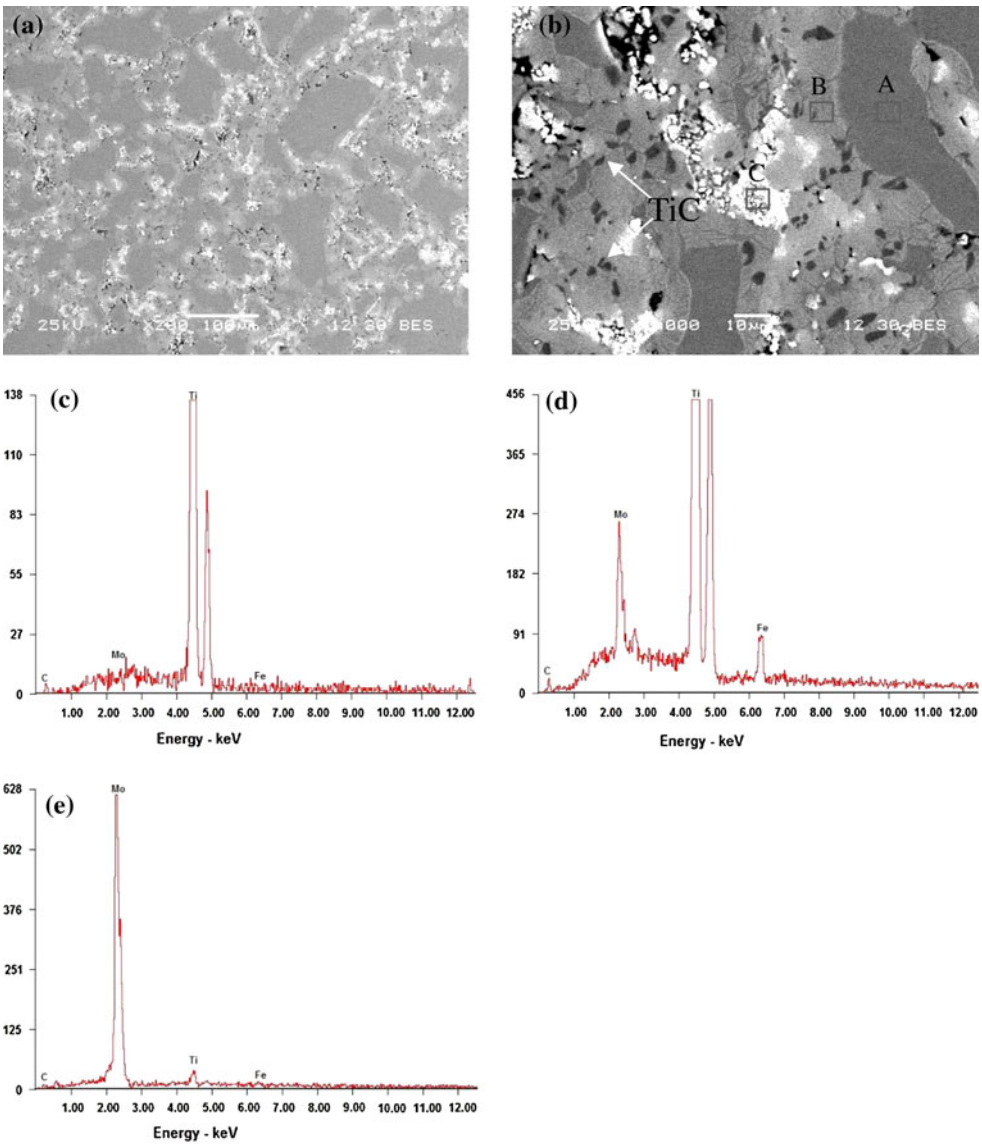

Fig. 4 **a**, **b** SEM pictures of Ti + Mo_2C compact sintering at 850 °C for 1.5 h; **c**–**e** corresponding energy spectra from EDS measurements in (**b**) marked as *A*, *B*, and *C*, respectively

instantaneous reactions between Ti and metal carbides (Mo_2C or VC). There is also no apparent endothermic event related to Fe–Ti or more complex C–Fe-M(Mo or V)–Ti liquid formation. This is in agreement with the results of [3] and the phase diagrams of Ti–Mo–C and Ti–V–C systems [15, 16]. However, both the curves change from endothermic to exothermic at about 600 °C, indicating both reactions can carry out in a wide range of temperatures. Hence, the reactions of Ti and metal carbide (Mo_2C or VC) compacts start at a very low temperature, and may proceed via a solid state reactive diffusion mechanism. According to the phase diagrams [17], continuous solid solutions will form in Ti–Mo and Ti–V systems, and carbon has a fixed solution concentration of about 0.5 wt% in Ti at elevated temperatures. Additionally, the diffusion coefficients of carbon, Mo, and V in Ti at 1300 °C were reported to be approximately in the magnitudes of $10^{-6.5}$, 10^{-13}, and 10^{-13} $m^2\ s^{-1}$, respectively [18–20], and the diffusion coefficients of Ti in Mo or V at the same temperature was approximately in the magnitude of 10^{-16} $m^2\ s^{-1}$ [19, 20]. Therefore, at the first stage of both reactions, the components M (Mo or V) and carbon of the metal carbides are dissolved in Ti, leading to the formation of a Ti–M(C) solute in the Ti particle surface. When there is a sufficiently high content of carbon and M in Ti particles, TiC phase precipitates from the Ti–M(C) solid solute. A two-phase reaction zone consisting of the Ti–M(C) matrix and the TiC particles is thus formed between Ti and metal carbides, as shown in Figs. 4 and 6. It is suggested that the competitive demand for carbon atoms occurs between the growth of the two-phase reaction zone and the precipitation of TiC during the reactions, and has a great influence on the nucleation and growth of TiC particles.

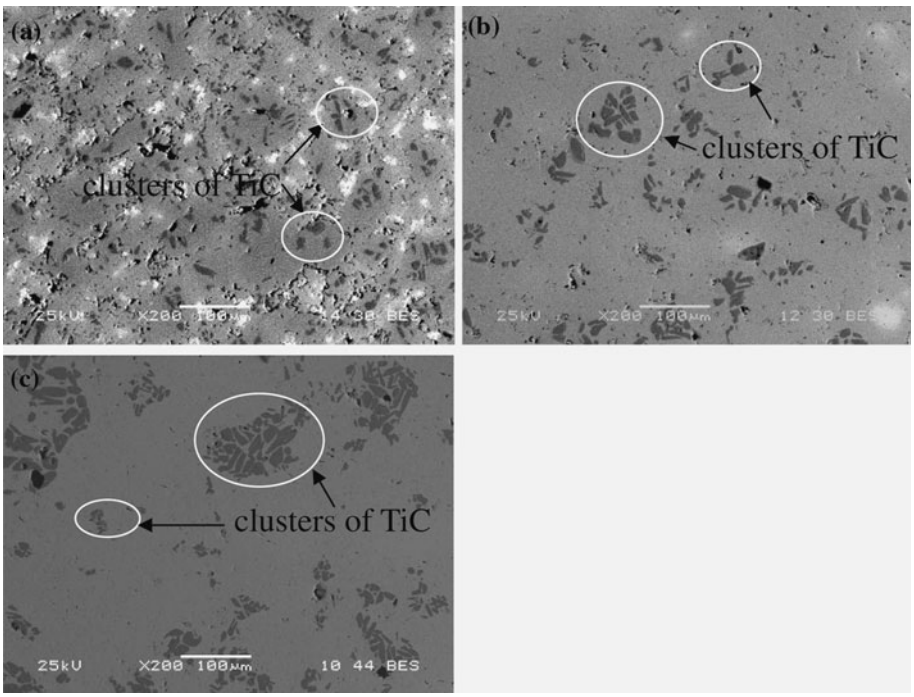

Fig. 5 SEM pictures of Ti + Mo_2C compacts sintering for 1.5 h at: **a** 1000 °C, **b** 1150 °C, and **c** 1300 °C

Based on the model proposed by Paransky [21], the mass balance requirement for the carbon component in the Ti–M(C) matrix and in the TiC particles can be described as follows:

$$w = K_R C(1-f) \tag{3}$$

$$\frac{\partial(C(1-f))}{\partial t} = -K_R C(1-f) + \frac{\partial}{\partial x}\left[D_{\text{eff}}\frac{\partial C}{\partial x}\right] \tag{4}$$

where w is the amount of carbon atoms transferred from the matrix to the TiC phase per unit volume, c is the concentration of carbon in Ti(C, M); K_R is the reaction rate constant, a phenomenological coefficient to describe the overall precipitation process of TiC, including nucleation and growth of new TiC particles, f is the volume fraction of the TiC precipitate, and D_{eff} is the effective diffusion coefficient in the two-phase layers. The driving forces for reaction between Ti and metal carbide may be different in the case of Mo_2C and VC, and induce a higher reaction rate in the Ti + Mo_2C compact than in the Ti + VC compact. It can be demonstrated by the co-existence of VC and TiC in the Ti + VC compact (Figs. 3, 6) after sintering at 850 °C for 1.5 h. According to Eq. 3, the volume fraction (f) of TiC particles increases with the increase of the reactive rate K_R, while keeping w and c as constants. It implies that the nucleation or growth of TiC precipitates can be enhanced by increasing the reaction rate. It was shown in [21] that increasing the reaction rate results in decreasing the maximum thickness of the two-phase layer according to Eq. 4. Therefore, it can be concluded that a high amount of TiC particles form in a thin thickness of a two-phase layer due to the fast reaction rate. Hence, clusters of TiC are present in the Ti + Mo_2C compact, as shown in Fig. 5. Decreasing the reaction rate would be in favor of the homogeneous diffusion of carbon and the nucleation of TiC in a wide range. Thus, a homogeneous distribution of TiC particles appears in the Ti + VC compact, as shown in Fig. 7.

Densification mechanism

As mentioned above, the reactions of Ti and metal carbide (Mo_2C or VC) compacts occur by a solid-state diffusion mechanism, and the densification process is also through a solid-state mass transformation. Factors that enhance the mass transfer in solid-state diffusion are helpful for accelerating the sintering of powder metallurgical Ti alloys. During the initial stage of sintering, a large volume of fresh surfaces of Mo and Ti is created due to intensive reaction between Ti and Mo_2C, promoting the onset of diffusion and the formation of sintering necks in the Ti + Mo_2C compact. During the following stage, the diffusion creep is suggested to be the controlling mechanism of the densification process [22]. It was reported [20] that the frequency factor (D_0) in Arrhenius equation ($D_{\text{inter}} = D_0 \exp(-Q/RT)$) increases with the increase of the Mo concentration in Ti (when Mo < 35 wt%). Additionally, more β phase is stabilized by the addition of Mo. β phase is known to be of much lower elevated temperature strength

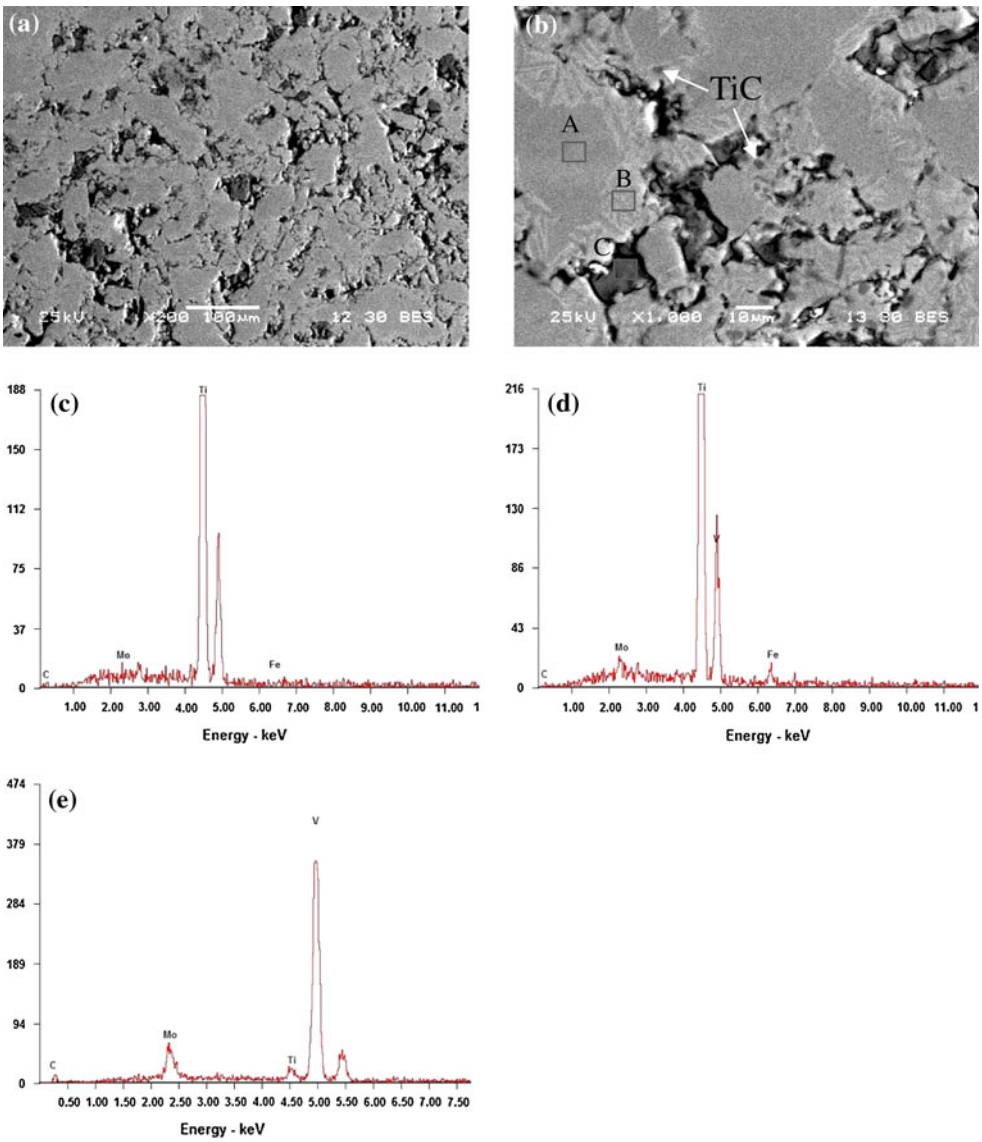

Fig. 6 **a**, **b** SEM pictures of Ti + VC compact sintering at 850 °C for 1.5 h; **c**–**e** corresponding energy spectra from EDS measurements in (**b**) marked as *A*, *B*, and *C*, respectively

than that of α phase. At constant sintering stress, the diffusion creep rate during the intermediate stage would be accelerated due to the good flow ability of β phase. Hence, a high relative density is achieved in the Ti + Mo_2C compact. The slow decomposition rate of VC powder particles might contribute to the slow densification process and low relative density of the Ti + VC compact.

Mechanical behavior

TiC particles and Ti(Mo or V) solid solution are formed in the Ti + Mo_2C and Ti + VC compacts after reactive sintering. It is indicated that TiC/Ti interfaces in the reactive sintered TiC/Ti composites have a good cohesion, because the cleavage is the main fracture mechanism for TiC particles, and the stress concentration loaded at the interfaces can be transferred from the Ti matrix to the TiC particles [23]. On the other hand, the Mo and V have a solid solution strengthening effect in the matrix. Therefore, reactive sintering of Ti and metal carbide compacts is a desirable way to fabricate in situ TiC/Ti composite. It is obvious that the molybdenum equivalency value of Ti + Mo_2C composite with 12 wt% Mo_2C addition is higher than that of Ti + VC composite with 6 wt% VC addition. The high strength of Ti + Mo_2C composite is mainly attributed to its high molybdenum equivalency value and less residual pores. Due to the deterioration effect of residual pores and the brittle fracture of TiC particles on the plastic deformation, both composites have a relatively low ductility.

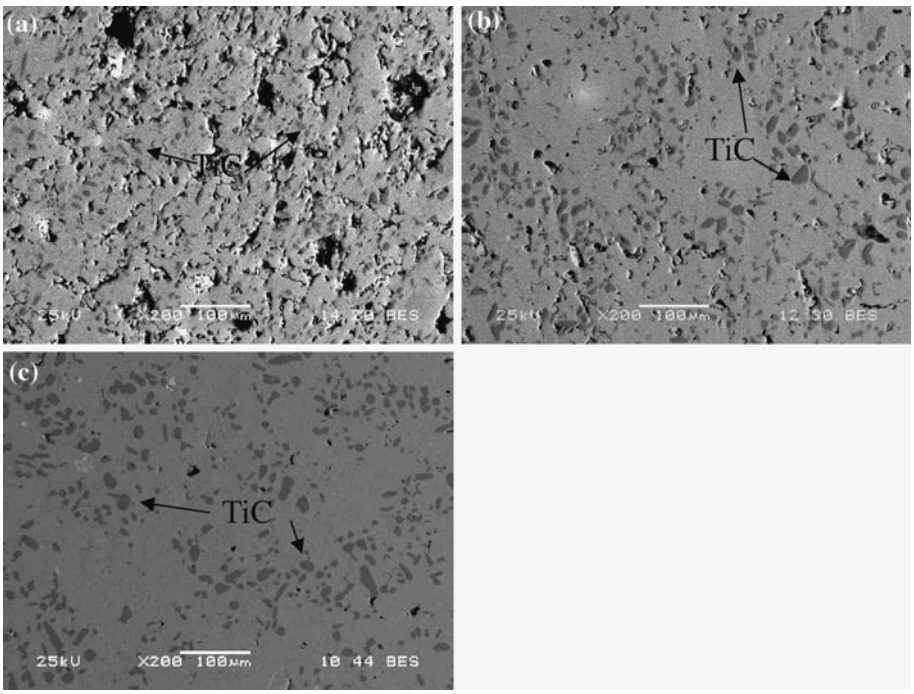

Fig. 7 SEM pictures of Ti + VC compacts sintering for 1.5 h at: **a** 1000 °C, **b** 1150 °C, and **c** 1300 °C

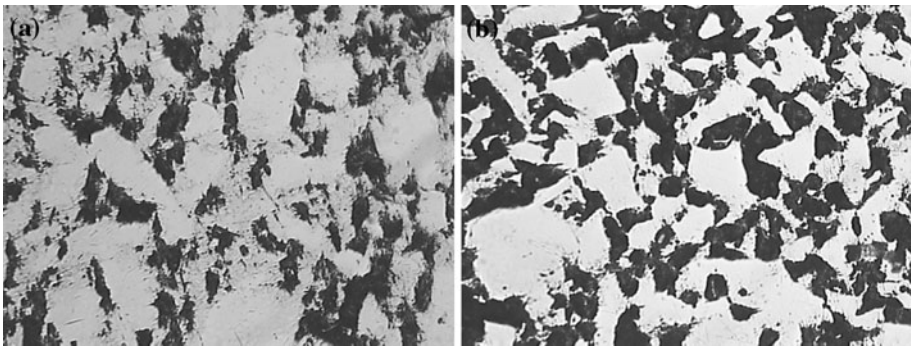

Fig. 8 Optical micrographs for **a** Ti + Mo_2C compact and **b** Ti + VC compact after sintering at 850 °C for 1.5 h

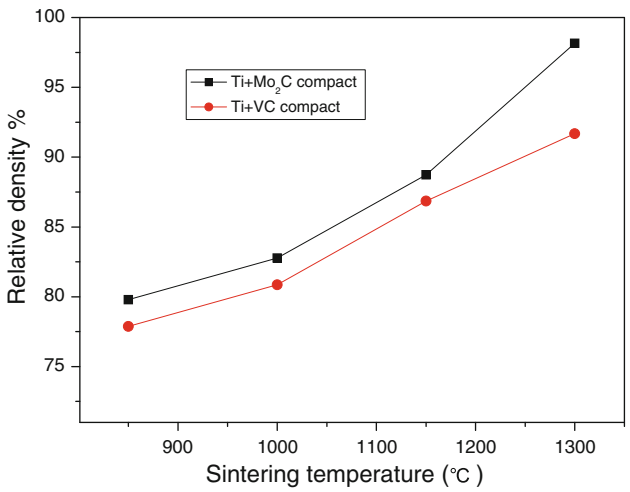

Fig. 9 Densities of Ti + Mo_2C and Ti + VC compacts after sintering at different temperatures for 1.5 h

Table 1 Mechanical properties of the composites after sintering at 1300 °C for 1.5 h

Titanium composites	Tensile strength (MPa)	Yield strength (MPa)	Elongation (%)
Ti + Mo_2C composite	834.5	827.8	4.6
Ti + VC composite	596.7	590.9	5.3

Conclusions

(1) The reactions of Ti and metal carbide (Mo_2C or VC) compacts occur via a solid-state reactive diffusion mechanism. The formation of a two-phase reaction zone, which consists of the Ti(M, C) matrix and the TiC precipitates, leads to the competitive demand for carbon between the growth of the interlayer and the precipitation of TiC.

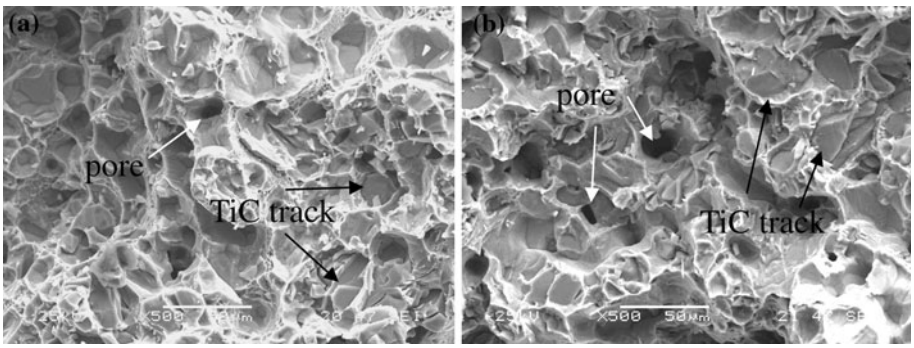

Fig. 10 Scanning electron micrographs of tensile fracture surface of the composites after sintering at 1300 °C for 1.5 h: **a** Ti + Mo_2C composite and **b** Ti + VC composite

(2) Due to the different rates of the carbon diffusion and the TiC formation, the TiC particles formed in the Ti + Mo_2C composite are denser and more inhomogeneously distributed than those in the Ti + VC composite.

(3) The TiC/Ti interfaces in the TiC/Ti composites show a good cohesion, and can transfer the stress from Ti matrix to TiC particles. The high strength of Ti + Mo_2C composite is attributed to its high molybdenum equivalency value and less residual porosity.

Acknowledgements This study is supported by the Minister of Science & Technology of China under contract No. 2007BAE07B05, the Graduate Degree Thesis Innovation Foundation of Central South University under the grant No. 1960-71131100005, and the Innovative Fund of the State Key Lab of P/M.

References

1. Gorsse S, Miracle DB (2003) Acta Mater 51:2427
2. Lu WJ, Zhang D, Zhang XN, Wu RJ (2001) Scripta Mater 44:2449
3. Liu Y, Chen LF, Tang HP, Liu CT, Liu B, Huang BY (2006) Mater Sci Eng A 418:25
4. Ni DR, Geng L, Zhang J, Zheng ZZ (2008) Mater Sci Eng A 478:291
5. Ranganath S, Subrahmanyam J (1996) Metall Mater Trans A 27:237
6. Ranganath S, Vijayakumar M, Subrahmanyam J (1992) Mater Sci Eng A 149:253
7. Vyas A, Rao KP, Prasad YVRK (2009) J Alloy Compd 475:252
8. Radhakrishna Bhat BV, Subramanyam J, Bhanu Prasad VV (2002) Mater Sci Eng A 325:126
9. Ni DR, Geng L, Zhang J, Zheng ZZ (2006) Scripta Mater 55:429
10. Liu HZ, Yao B, Wang LH, Wang AM, Ding BZ, Hu ZQ (1996) Mater Lett 27:183
11. Kim YJ, Chung H, Kang SJL (2001) Composites A 32:731
12. Liu B, Liu Y, He XY, Tang HP, Chen LF, Huang BY (2007) Metall Mater Trans A 38:2825
13. Hagiwara M, Arimoto N, Emura S, Kawabe Y, Suzuk HG (1992) ISIJ Int 32:909
14. Binnewies FM, Milke FE (2002) Thermochemical data of elements and compounds. Wiley-VCH, Weinheim
15. Bandyopadhay D, Haldar B, Sharma RC, Chakraborti N (1999) J Phase Equilib l20:332
16. Bandyopadhay D, Sharma RC, Chakraborti N (2000) J Phase Equilib l21:199
17. Murray JL (1987) Monograph series on alloy phase diagrams: phase diagrams of binary titanium alloys. ASM International, Metal Park
18. Arvieu C, Manaud JP, Quenisset JM (2004) J Alloy Compd 368:116
19. Liu YJ, Ge Y, Yu D, Pan TY, Zhang LJ (2009) J Alloy Compd 470:176
20. Liang F, Shan LJ, Lei H, Hui C, Wen CY, Lian Z (2009) Chin J Nonferrous Met 19:1766
21. Paransky Y, Klinger L, Gotman I (1999) Mater Sci Eng A 270: 231
22. Kang SJL (2005) Sintering: densification grain growth & microstructure. Elsevier Butterwoth-Heinemann, Oxford
23. Tsang HT, Chao CG, Ma CY (1996) Scripta Mater 35:1007